J. Ind. Geophys. Union (January 2019)
v.23, no.1, pp: 41-54

Dimensionality and directionality analysis of the magnetotelluric data along the coastal part of western Saurashtra, Gujarat

K. Dilip Singh*, Kapil Mohan, and Mehul Nagar
Institute of Seismological Research, Raysan, Gandhinagar-382009 (Gujarat)
Also at Gujarat University, Navrangpura, Ahmedabad, Gujarat, 380009.
* Corresponding Author: ds200705@gmail.com

ABSTRACT
The Magnetotelluric (MT) data from 14 MT stations along a NW-SE profile, having a length of 40 km, is processed for a period range of 0.01-100s along the coastal part of north-western Saurashtra, India to estimate the dimensionality of the MT data, using three different approaches, that is, Phase Tensor (PT) technique, WALDIM code, Swift's and Bahr's Skew technique. The Swift's and Bahr's skew result suggests 1D structure for low periods (0.01-1 s) and 2D structure for high periods (1-100 s), except for some sites which show a 3D subsurface structure for high periods (1-100 s). The results generated through PT and WALDIM code are consistent with those from Swift's and Bahr's skew technique. The strike estimated through Phase Tensor (PT), Groom-Bailey (GB) and Becken and Burkhardt (BB) technique for broad period 0.01-100s suggest NNE-SSW regional strike direction, which is well correlated with the Delhi-Aravalli tectonic trend. From the 1D inverse model, the Quaternary and Tertiary sediments are found up to the depth of 300-400m followed by Deccan Trap. A conductive zone (having resistivity <20 Ohm-m) in the central part of the profile near Okha Rann is also observed which suggests the presence of a fault.

Keywords: Magnetotellurics, Dimensionality, Strike, Galvanic distortion, Western Saurashtra coast, Gujarat

INTRODUCTION

Gujarat state is divided into three regions namely, Mainland Gujarat, Kachchh and Saurashtra on the basis of seismotectonics and geomorphology of the region (Yadav et al., 2008). The Saurashtra region comes under two seismic zones (IV and III) on the seismic zoning map of India (BIS, 2002). The major portion of the Saurashtra peninsula is covered by Arabian Sea water. The interior of the Saurashtra is either covered by Deccan Traps or Quaternary deposits due to which no clear faults have been identified. Various geophysical studies have been carried out in the Saurashtra region for regional as well as local tectonic interpretation. From Gravity and Magnetic method, Mishra et al. (2001) delineated major structural trends using satellite data: (i) NE-SW Precambrian Aravalli trend, observed in entire Saurashtra but dominating in the SE part of Saurashtra. (ii) ENE-WSW to E-W trend, which represents the Precambrian Son-Narmada lineament trend in southern Saurashtra. (iii) The NW-SE trend, parallel to the west coast of Saurashtra, visible over the entire Saurashtra peninsula. (iv) N-S to NNE-SSW trend dominating in the eastern part of Saurashtra close to the Cambay basin. In central northern part of Saurashtra a Magnetotelluric survey with 607 stations was carried out in grid by Sharma et al. (2004), which identified near-surface structural features: (i) a near N-S trending fault/fracture passing through Amreli to Chotila and (ii) a near NW-SE trending fault passing through west of Lalpur. Subbarao et al. (2012) recorded magneto-variational fields by an array of magnetometers covering whole Saurashtra region and inferred the presence of two prominent conductivity anomalies: (i) the first elongated anomaly coinciding with the horst and graben offshore structures of Saurashtra and Kachchh, and (ii) the second anomaly is found over the Saurashtra depression that correlates well with the low-magnetization anomaly extending in the NW-SE direction towards Cambay basin. From Deep Resistivity Sounding (DRS) data, Singh et al. (2004) generated a geo-electrical section of Navibandar-Rajkot-Dhrangadhra and observed the resistivity of sediments less than 60 ohm-m, traps of 100-600 ohm-m and basement of >1000 ohm-m. The presence of the number of hidden volcanic plugs in the area of Porbandar-Navibandar, Kutiyana, Junagadh and, Rajula region are observed in which some plugs are not exposed at the surface and could be an extension of Girnar, Barda and Alech hills at depth. Patro et al., 2015 have acquired a N-S profile across the center of the Saurashtra and correlated the velocity model from the seismic study with the resistivity model generated from MT data and observed that velocity of different layers increases with increase in resistivity of the different layers. From MT data analysis the resistivity of 120 ohm-m, 20 ohm-m and >1000 ohm-m were found for Deccan trap, Mesozoic sediments, and basement rock respectively.

In a nutshell, most of the geophysical study has been conducted in the Southern and central part of the Saurashtra. The NW Saurashtra has not been covered with geophysical survey. Therefore, the MT survey was planned in the NW part of Saurashtra to understand the dimensionality, directionality and the conductivity variations in the subsurface. Total 14 MT stations have

Table 1. Lithostratigraphy of Neogene-Quaternary deposits of Saurashtra region (Bhatt, 2000 and Pandey et al., 2007)

Stratigraphic Unit	Lithology	Age
Holocene Deposits	Beach and dune sands Tidal clays, alluvium	Holocene
Unconformity		
Chaya Formation	Calc-rudite, Calc-arenites	Late Pleistocene to Holocene
	Coral reef limestone Off-white colored bioclastic limestone & conglomerate	Middle to Late Pleistocene
Unconformity		
Dwarka Formation	Recrystallized fossiliferous limestone and sandy Limestone	Lower Pliocene
	Sandy clays and sandstones	Upper Miocene
	Bioclastic and coralline limestone with few dolomitic bands	Middle Miocene
Disconformity		
Gaj Formation	Yellow and brown fossiliferous limestone	Lower to Middle Miocene
Deccan Trap	Basalt and other derivatives covered at places by laterite and bauxite	Upper Cretaceous to Eocene

been acquired. The MT data of 13 stations were used for further analysis and one station is rejected due to presence of high-level noise in the data. The dimensionality analysis has been carried out using Swift skew (Swift, 1967); Bahr skew (Bahr, 1988, 1991); Phase Tensor Analysis (PTA) (Caldwell, 2004), WALDIM decomposition technique (Marti et al., 2009). The strike analysis has been carried out using Multisite Multifrequency tensor decomposition (McNeice and Jones, 2001; Becken and Burkhardt, 2004).

GEOLOGY AND TECTONICS

The Saurashtra region is a horst structure (Biswas, 1982), bounded by the Cambay Rift Basin (CRB) in the east, West Coast Fault (WCF) in the west, extension of Son Narmada Fault in the south and North Kathiawar Fault (NKF) in the north (Figure 2). Major geological and tectonic events of the Saurashtra region are narrowed to Mesozoic and Cenozoic era and associated with (i) break-up of Africa from the Indian block containing Madagascar and Seychelles, (ii) later breakup of Madagascar from India due to Marion hotspot activity, and (iii) break-up of the Seychelles plateau from India followed by eruption of Deccan volcanism related to interaction of Reunion hotspot activity (Subbarao et al., 2012). The region has observed various tectonic activities such as deviational forces causing inter-continental splitting, different phases of rifting, re-activation of the ancient fault zones and Deccan volcanism due to reunion plume activity. Major continental part is covered with the Deccan trap. The coastal plains fringing the trappean highland comprise Cenozoic cover consisting of Tertiary and Quaternary sediments (Biswas, 1987). The Tertiary exposures are patchy in occurrence and mostly belong to Dwarka Formation (Bhatt, 2000) (Figure 1). A thin cover of Neogene and Quaternary sediments occurs at the top surface (Table 1).

Magnetotelluic data and processing

Magnetotelluric (MT) data at 14 stations are acquired along the NW-SE traverse of ~40 km with ~3 km station spacing. The MT data acquisition system ADU-07e of M/s Metronix, Gmbh, Germany was deployed. The data was measured for five components, using induction coils (MFS-06) for three orthogonal channels of magnetic field variation (Hx, Hy, and Hz) and Pb-$PbCl_2$ electrode dipoles (80m dipole length) for orthogonal electric field variations (Ex and Ey). The MT data were recorded for about 48 hours over a broad period range. The time series data were processed using a software package Mapros to estimate the apparent resistivity and phase curves (Figure 3).

METHODOLOGY

In MT method, the horizontal Electric fields (**E**) and the horizontal magnetic fields (**B**) are linked through a

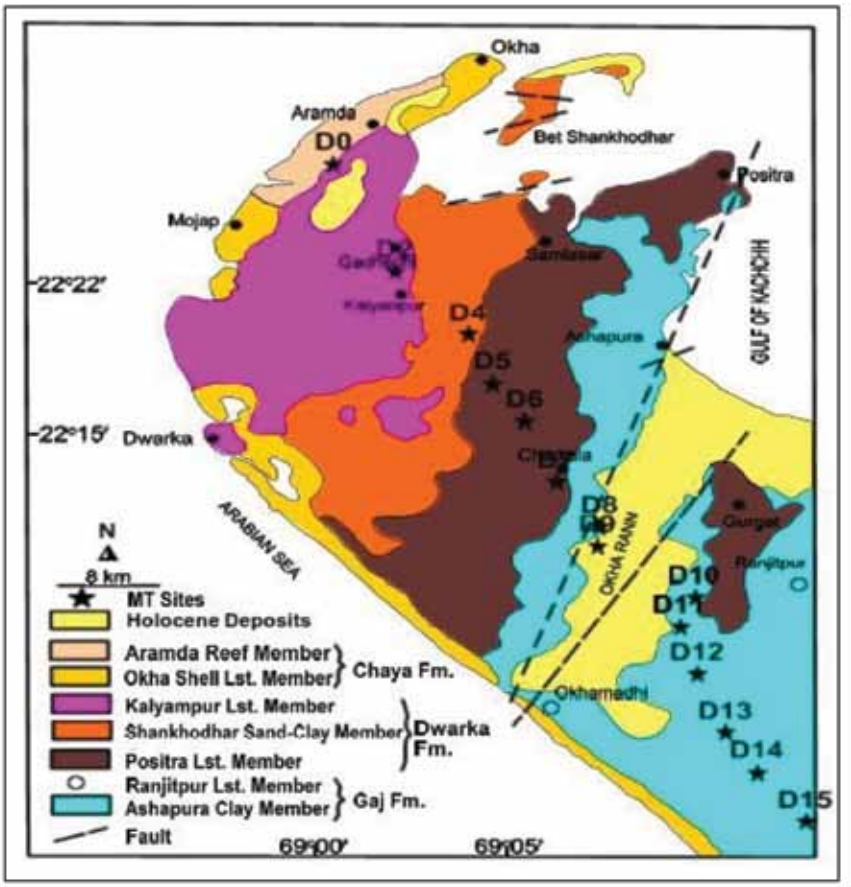

Figure 1. Geological Map of the study area of the Saurashtra region (Gujarat), along with Magnetotelluric Stations marked in black star symbol (modified after Bhatt, 2000).

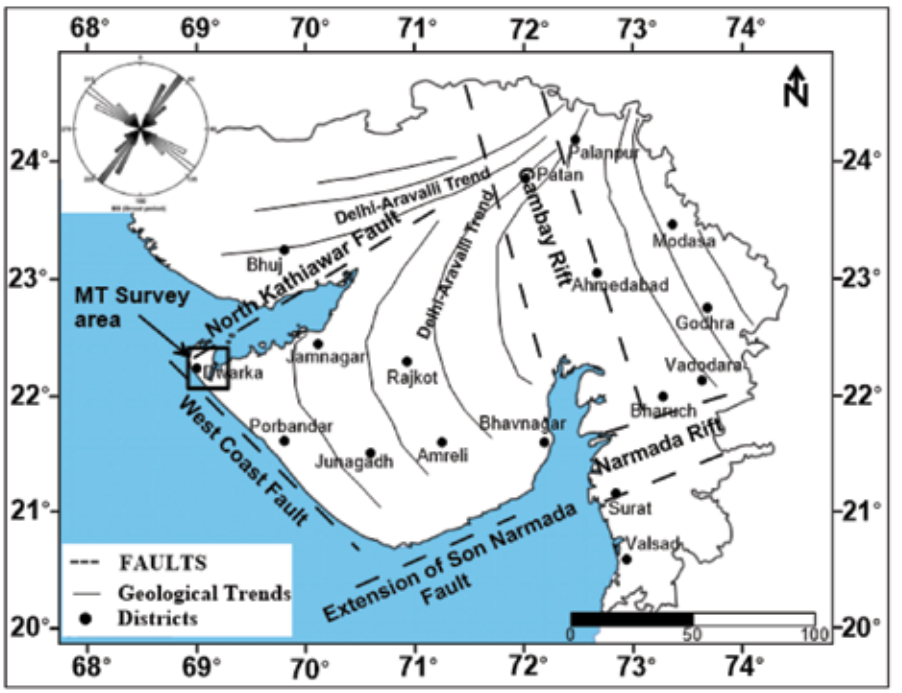

Figure 2. Tectonic Precambrian trend (after Biswas, 2005) along with regional strike direction estimated through BB technique.

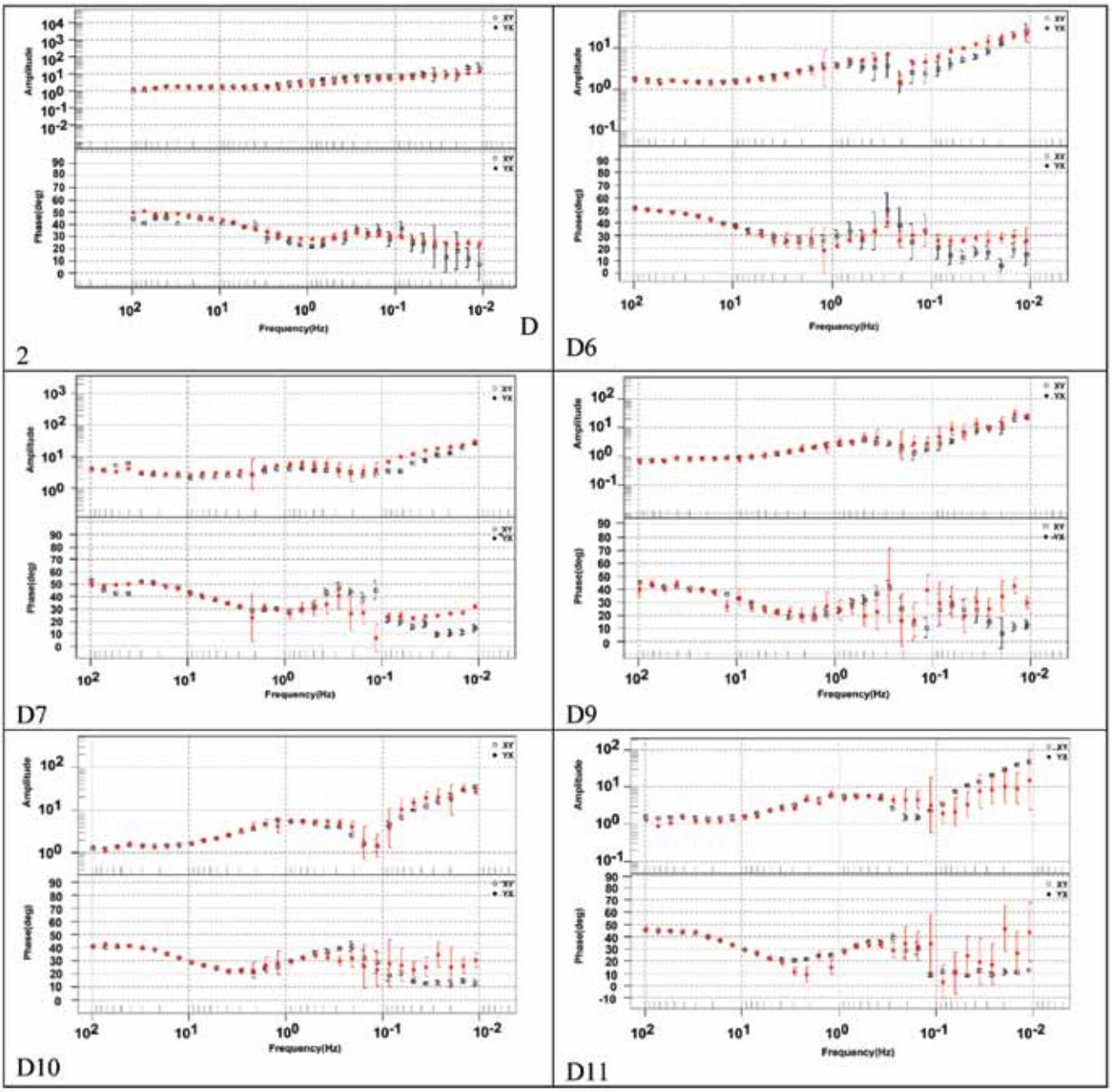

Figure 3. Computed apparent resistivity and Phase Vs. Frequency curves after time-series processing.

complex impedance tensor **Z** (Bahr, 1988) in the frequency domain:

$$E = Z.B$$

$$Z = \begin{pmatrix} Z_{xx} & Z_{xy} \\ Z_{yx} & Z_{yy} \end{pmatrix}$$

Swift skew

Swift's skew indicates the dimensionality of the subsurface structure (Swift, 1967). This is independent of rotation of the tensor matrix and the values ranges generally from 0 to 0.5 (Vozoff, 1972). The values are less than 0.2 for 1-D and 2-D structures (Swift, 1967). Higher skew values indicate the more complex structure of the site. In some cases, apparent resistivity and phase may be well-behaved but skew will show a high value if 3-D inhomogeneity is present (Berdichevsky, 1999). Skew measures impedance components differences to find out the deviation from 2-D structures (Swift, 1967). The diagonal terms are influenced strongly by noise. Consider the modified impedances.

$$S_1 = Z_{xx} + Z_{yy},$$
$$S_2 = Z_{xy} + Z_{yx},$$
$$D_1 = Z_{xx} - Z_{yy},$$
$$D_2 = Z_{xy} - Z_{yx}$$

Where, S1 and D1 are rotationally invariant.

Further, Swift's skew is defined as,

$$K = \left|\frac{S_1}{D_2}\right|$$

Bahr skew

Bahr's skew (BS) is a measure of the local 3-D distortion of regional 2-D fields based on impedance phase, rather than on impedance magnitudes that is the conventional definition of skew (Vozoff, 1972). For BS greater than 0.3 the data considered as 3-D (Bahr, 1991). The Bahr's skew is given as:

$$\eta = \frac{\left(\left[D1, S2\right] - \left[S1, D2\right]\right)^{1/2}}{\left|D_2\right|}$$

Where, D_1, D_2, S_1 and S_2 are derived in above equations.

Extended Groom and Bailey decomposition

Extended Groom and Bailey decomposition method (McNeice and Jones, 2001) has been used to find the most consistent 2-D parameters over a different frequency band. Extended GB decomposition (McNeice and Jones, 2001) utilizes all the physical constraints implicit to the Groom Bailey decomposition model (Groom and Bailey, 1989) which imposed simultaneously on all dataset and a global minimum misfit solution achieved to estimate a regional geo-electrical strike in presence of galvanic 3-D distortions. This decomposition technique shows shear and twist values. If the values are above +/-45 for shear and twist, the data is 3D in nature.

Phase tensor analysis

The invariant parameters lambda and beta determine the dimensionality of regional impedance tensor (Bibby et al., 2005 & Caldwell et al., 2004). Bibby (2005) distinguished 1-D, 2-D and 3-D structures on the values of lambda and beta. In case of 1-D structure, the lambda as well as beta will be zero, for 2-D structure lambda become non-zero, while the beta become zero and for 3-D structure both beta as well as lambda become non-zero. The criterion provided by the phase tensor parameters is necessary but not sufficient for determining the dimensionality of the regional conductivity structure (Bibby et al., 2005). The dimensionality evaluated using phase tensor gives the best result by considering the MT sites from different locations collectively. It has become common practice to combine the problem of determining the strike direction with distortion removal. The phase tensor provides the better solution for dimensionality and the strike direction. The Phase Tensor is defined as,

$$\phi = X^{-1} \quad Y$$
$$\phi = \left(DX_R\right)^{-1}\left(DY_R\right)$$
$$\phi = X_R^{-1} D^{-1} DY_R$$
$$\phi = X_R^{-1} Y_R = \phi_R$$

Where, Φ & ΦR are measured and regional phase tensors, D is distortion tensor, X and Y are real & imaginary parts of the measured impedance tensor, X_R and Y_R are real and imaginary parts of regional impedance tensor.

The following equations derive the formulae of Lambda and Beta:

$$\phi = \begin{bmatrix} X_{22}Y_{11} - X_{12}Y_{21} & X_{22}Y_{12} - X_{12}Y_{22} \\ X_{11}Y_{21} - X_{21}Y_{11} & X_{11}Y_{22} - X_{21}Y_{12} \end{bmatrix} \Big/ \det(X)$$
$$\phi = \begin{bmatrix} \phi_{11} & \phi_{12} \\ \phi_{21} & \phi_{22} \end{bmatrix}$$

Where, det(X) = $X_{11}X_{22} - X_{21}X_{12}$

The simplest algebraic representations of the tensor invariants are the trace

$$tr(\phi) = \phi_{11} + \phi_{22}$$

The skew is:

$$sk(\phi) = \phi_{12} - \phi_{21}$$

and the determinant of the matrix is:

$$\det(\phi) = \phi_{11}\phi_{22} - \phi_{12}\phi_{21}$$

The first order function of all the invariants is:

$$\phi_1 = \frac{tr(\phi)}{2}$$
$$\phi_2 = \left[\det(\phi)\right]^{1/2}$$

and

$$\phi_3 = \frac{sk(\phi)}{2}$$
$$\phi_{\min} = \left(\phi_1^2 + \phi_3^2\right)^{1/2} - \left(\phi_1^2 + \phi_3^2 - \phi_2^2\right)^{1/2}$$
$$\phi_{\max} = \left(\phi_1^2 + \phi_3^2\right)^{1/2} + \left(\phi_1^2 + \phi_3^2 - \phi_2^2\right)^{1/2}$$
$$Ellipticity(\lambda) = \frac{(\phi_{\max} - \phi_{\min})}{(\phi_{\max} + \phi_{\min})}$$
$$Skew(\beta) = \frac{1}{2}\tan^{-1}\left(\frac{\phi_3}{\phi_1}\right)$$

Therefore, PT ellipses can be plotted by obtaining values from Ellipticity (λ) and Skew angle (β).

Table 2. Estimated PT ellipse parameters for different periods at each site.

Periods	PT Ellipse Parameters	D2	D4	D5	D6	D7	D8	D9	D10	D11	D12	D13	D14	D15
0.1s	Beta	0.0	1.9	-1.9	-0.1	4.2	-0.7	-7.3	-0.6	1.6	0.4	2.7	0.2	0.4
	Phimin	0.8	0.7	0.7	0.7	0.9	1.1	0.6	0.5	0.5	0.5	0.5	0.4	0.4
	phimax	0.9	0.8	0.8	0.8	0.9	1.1	0.7	0.6	0.6	0.6	0.5	0.5	0.4
1s	Beta	2.1	-1.7	-2.9	-0.3	-3.5	4.6	-2.3	1.4	1.2	0.8	-5.1	3.0	5.6
	Phimin	0.4	0.5	0.5	0.4	0.5	0.6	0.4	0.5	0.5	0.6	0.5	0.5	0.6
	phimax	0.5	0.5	0.8	0.6	0.5	0.6	0.5	0.6	0.5	0.7	0.7	0.8	0.8
10s	Beta	-6.0	7.2	-42	-15	3.7	2.4	-5.4	6.5	41	-32	-0.9	-40	41
	Phimin	0.4	0.4	0.5	0.2	0.2	0.3	0.2	0.2	-0.1	-0.0	0.3	0.0	0.3
	phimax	0.8	0.8	0.9	0.7	0.8	0.8	1.3	1.3	0.8	0.2	1.2	0.7	0.9
100s	Beta	5.8	3.8	26	-17	5.2	7.0	5.7	7.6	2.4	-27	-1.8	-32	4.0
	Phimin	0.1	0.3	0.3	0.2	0.2	-0.2	0.2	0.2	0.2	0.2	0.1	0.4	0.5
	phimax	0.5	0.5	2.9	0.6	0.9	0.5	0.7	0.8	2.8	0.8	0.7	1.1	1.1

Induction Arrows

Induction arrows are vector representations of the complex ratios of vertical to horizontal magnetic field components (Naidu, 2012). It determines the presence or absence of lateral variations in conductivity (Jupp and Vozoff, 1976). In a 2-D Earth, induction arrow is associated only with the E-polarization. Thus, insulator conductor boundaries extending through a 2-D Earth gives rise to induction arrows that orient perpendicular to them and their magnitude indicate the intensities of anomalous current concentrations (Wiese, 1962). The vectors point towards the anomalous internal concentrations of current (Simpson and Bahr, 2005) called Parkinson convention, whereas the vector points away from the internal current concentrations are called Wise convention

WALDIM Technique

WALDIM, a FORTRAN code is used to perform the dimensionality analysis of Dwarka MT data. This code is based on Weaver et al. (2000) criteria. WALDIM technique allows categorizing the dimensionality into bands of periods for each site, in order to have a more stable estimate of the dimensionality. For particular site and their frequency, the code figures the type of dimensionality structure, as well as, strike direction and distortion parameters, including errors. This method of averaging over period bands differs from that used in the Strike Decomposition code, with the main difference that, whereas Strike Decomposition code provides least-squares fit to data from a given period band, however WALDIM averages the separate results within the band. Weaver et al. (2000) presented a dimensionality study based on sets of rotationally invariant scalars computed from the observed MT impedance tensor. The set of eight invariants (i.e. seven independent (I1, I2, I3, I4, I5, I6, I7) and a dependent one (Q)) known as WAL invariants, defined in a way that the invariants represent a Mohr circle diagram. The I1 and I2 are non-dimensional and normalized to unity, their vanishing has a physical interpretation, specifically related to the geoelectric dimensionality. Based on these WAL invariants, Marti et al. (2009) developed a code for dimensionality analysis known as WALDIM. This provides a robust description of the subsurface dimensionality, as well as the parameters necessary for data correction prior to model.

RESULTS AND DISCUSSIONS

To obtain dimensionality information of the regional subsurface structure the Swift's skew and Bahr's skew are computed for a period range of 0.01-100 s, at all stations (Figure 4). The Swift's skew values have been found less than 0.2° at majority stations for period range 0.01-100 s, which suggests the 1D and 2D nature of the structure, but at some stations the Swift's skew plot shows higher value (i.e. > 0.2°) for period range 10-100s, indicating the 3D subsurface structure. The Bahr's skew plot shows a value less than 0.3° for period range of 0.01-100s, which suggests the structure, is 1D and 2D, but at some sites, the value rises above 0.3° for period range 10-100s, indicating the structure is 3D. Patro et al., (2005), Tao et al., (2010), Naidu et al., (2011), Hubert, (2012), Barcelona et al., (2013), Oskooi et al., (2013) and Pranata et al., (2017) have also applied these techniques in the past.

Phase tensor ellipse calculated for the four different periods (0.1, 1, 10 and 100 sec) are presented in Figure 5. As stated earlier, Bibby, (2005) distinguished 1D, 2D and 3D structures based on lambda and beta values. Referring to the criteria given by Bibby (2005), the calculated phase tensor ellipses for 0.1sec and 1sec are close to circular, which indicates the 1D subsurface structure. The ellipses

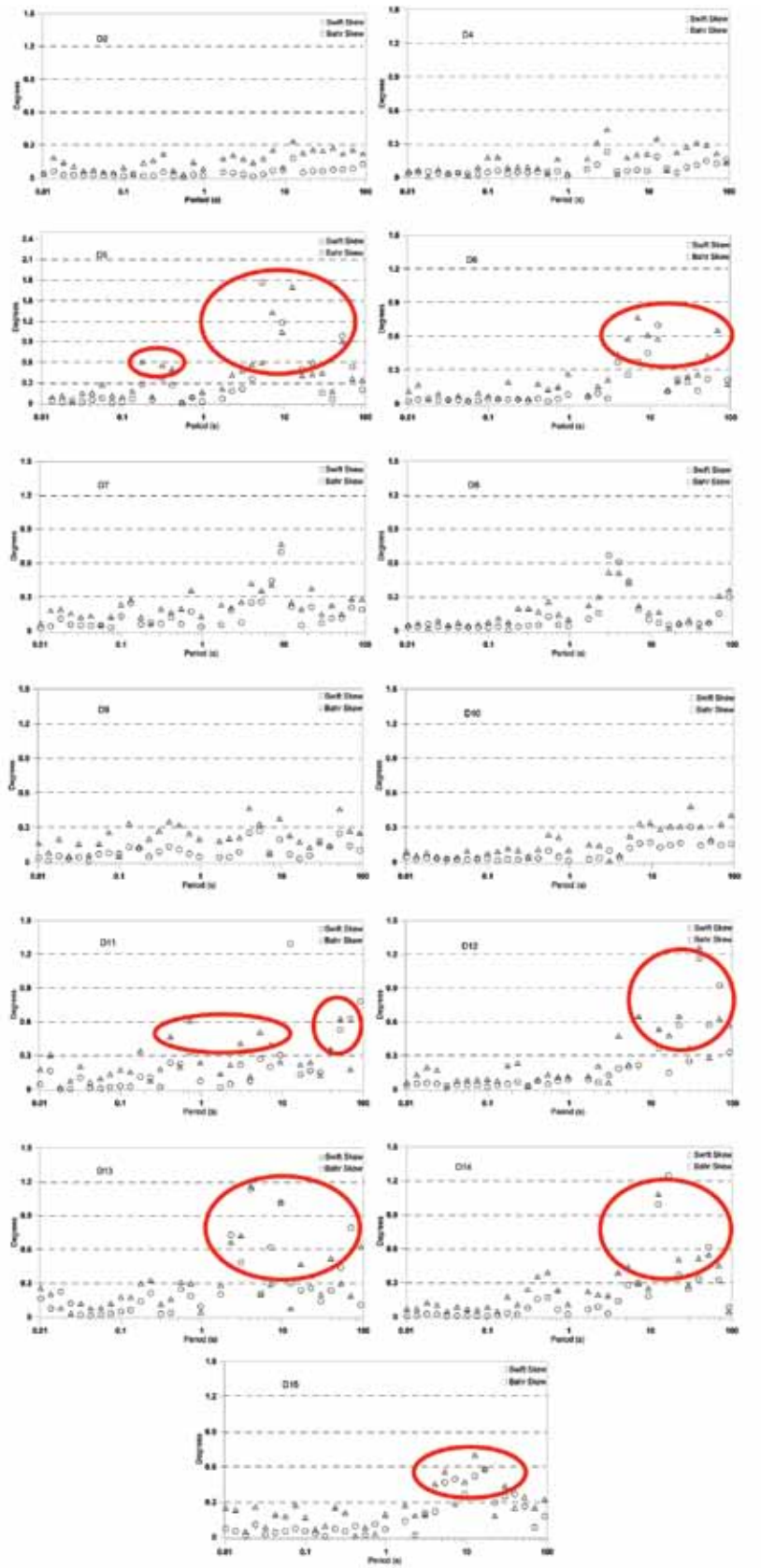

Figure 4. Swift's and Bahr's skew plots showing 3D effects (data points marked with red circles) for periods greater than 1 sec.

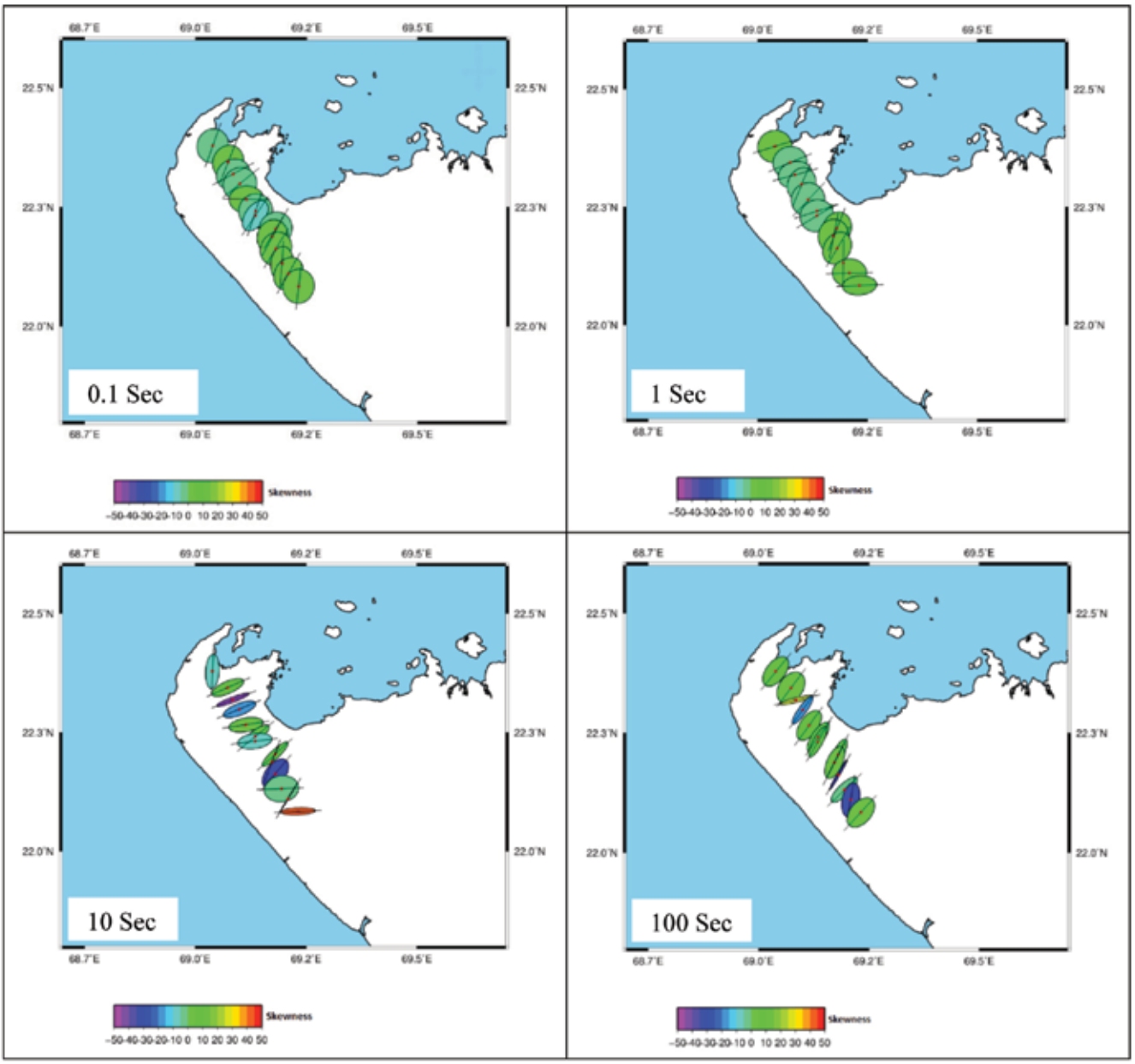

Figure 5. Phase Tensor Ellipse plots along the MT profile for four different periods (0.1, 1, 10 and 100 Secs).

at 10secs and 100secs are elongated, suggesting the 2D structure. At some stations, the plot shows high skew values which indicate 3D subsurface structure. The major axes of the ellipses are aligned mainly in NNE-SSW direction, which is consistent with the structural trend shown in Figure 2. The estimated values of major axes, minor axes and beta are mentioned in Table-2. Heise et al., (2008), Tao et al., (2010), Selway et al., (2012), Booker, 2014, Febriani et al., (2017) and Pranata et al., 2017 employed the phase tensor technique in their study to estimate the dimension of the subsurface structure.

According to Jones and Groom (1993), the proper selection of strike angle is important as it represents the structure in the model calculated from MT data and if the strike angle chosen is incorrect, it will lead to erroneous model. The choice of strike angle can be done by geological/tectonic trends of the region. There are several ways to estimate strike direction. In the present study, strike direction for broad period as well as various period bands is estimated through Phase Tensor (PT), Groom-Bailey (GB) and Becken and Burkhardt (BB) techniques (Figure 6). The NNE-SSW strike direction has been estimated in the

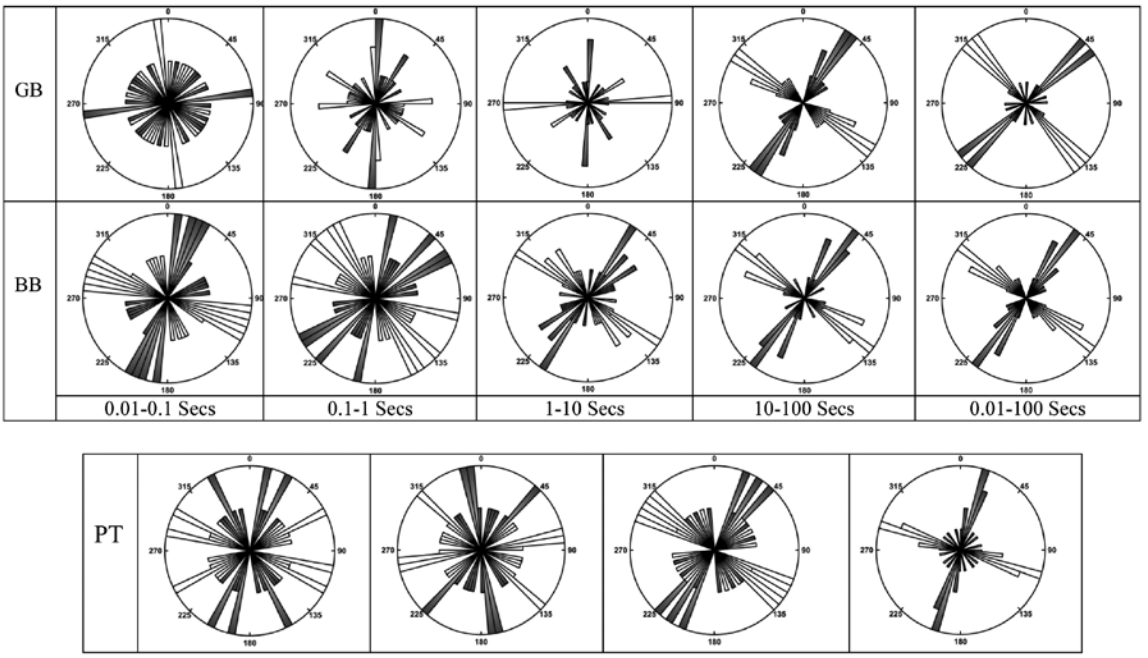

Figure 6. Rose diagram plot of regional strike direction for broad period through Groom-Bailey Decomposition (GBD), Becken and Burkhardt Decomposition (BBD) and phase tensor (PT) techniques.

Table 3. Strike values estimated for broad period range through three techniques (GB, BB and PT)

Sites	GB (0.01-100s)	BB (0.01-100s)	PT(100s)
D2	54.7	37.8	18.55
D4	73.1	36.6	08.00
D5	40.4	57.3	16.08
D6	39.5	27.1	16.56
D7	43.6	35.5	21.91
D8	51.9	38.0	-14.24
D9	0.00	30.1	20.15
D10	42.6	28.5	21.29
D11	34.8	48.3	16.82
D12	43.6	20.6	01.75
D13	54.7	45.5	08.57
D14	45.5	27.0	-39.25
D15	51.3	67.0	37.73

area, which is in good agreement with the tectonic trend (Figure 2). The regional strike values are given in Table 3 for broad period range estimated through GB, BB and PT technique. Earlier, Patro et al. (2005) (BB technique); Naidu et al., 2011 (GB technique) and Barcelona et al., 2013 (GB technique), adopted these techniques in their study for the estimation of regional strike direction.

The dimensionality analysis has been conducted using WAL rotational invariants criteria the WALDIM code (Marti et al., 2009). The WALDIM code estimates the dimensionality in to period bands at each site. For each site the dimensionality of the band is the most occurring dimensionality response of the data in the band, if there occurs more than one dimensionality type in the band, priority is given to the lowest dimensionality. The dimensionality in the lower periods (0.0102 – 0.8286 sec) has been found 1D, except stations D12, D13, D14 and D15 (showing 3D and undetermined). The undetermined dimensionality is caused due to presence of error bars of the invariants Marti et al., 2009, while for higher periods (1.1110 – 90.4510 sec), it shows 3D/2D and 3D dimensionality at all stations (Table-4). Several researchers

Table 4. Dimensionality Analysis using WALDIM technique.

Sites	bands	Tmin.	Tmax.	Dimensionality	Sites	bands	Tmin.	Tmax.	Dimensionality
D2	1	0.0102	0.0793	1D		4	11.6078	90.4510	3D
	2	0.1063	0.8286	1D	D10	1	0.0102	0.0793	1D
	3	1.1110	8.6570	3D/2D		2	0.1063	0.8286	1D
	4	11.6078	90.4510	3D		3	1.1110	8.6570	3D
D4	1	0.0102	0.0793	1D		4	11.6078	90.4510	3D
	2	0.1063	0.8286	1D	D11	1	0.0102	0.0793	1D
	3	1.1110	8.6570	3D		2	0.1063	0.8286	1D
	4	11.6078	90.4510	3D		3	1.1110	8.6570	3D
D5	1	0.0102	0.0793	1D		4	11.6078	90.4510	UNDETERMINED
	2	0.1063	0.8286	1D	D12	1	0.0102	0.0793	1D
	3	1.1110	8.6570	UNDETERMINED		2	0.1063	0.8286	3D
	4	11.6078	90.4510	3D		3	1.1110	8.6570	3D
D6	1	0.0102	0.0793	1D		4	11.6078	90.4510	3D
	2	0.1063	0.8286	1D	D13	1	0.0102	0.0793	3D
	3	1.1110	8.6570	UNDETERMINED		2	0.1063	0.8286	3D
	4	11.6078	90.4510	3D		3	1.1110	8.6570	UNDETERMINED
D7	1	0.0102	0.0793	1D		4	11.6078	90.4510	UNDETERMINED
	2	0.1063	0.8286	3D	D14	1	0.0102	0.0793	1D
	3	1.1110	8.6570	1D		2	0.1063	0.8286	3D
	4	11.6078	90.4510	3D		3	1.1110	8.6570	3D
D8	1	0.0102	0.0793	1D		4	11.6078	90.4510	3D
	2	0.1063	0.8286	1D	D15	1	0.0102	0.0793	1D
	3	1.1110	8.6570	3D		2	0.1063	0.8286	3D
	4	11.6078	90.4510	3D/2D		3	1.1110	8.6570	UNDETERMINED
D9	1	0.0102	0.0793	1D		4	11.6078	90.4510	3D
	2	0.1063	0.8286	3D					
	3	1.1110	8.6570	UNDETERMINED					

have used this technique in their study for dimensionality analysis (Marti et al., 2010; Tao et al., 2010; Barcelona et al., 2013; Marti et al., 2016 and Kashkouli et al., 2016.

The purpose of distortion decomposition is to separate local and regional parameters as much as possible under the assumption that the regional structure is at most 2D and the local structures cause only galvanic scattering of the electric fields (Groom and Bailey, 1989). According to groom and bailey (1989), a family of unit vectors of an electric field is given by a vector on the x-axis which is deflected clockwise by an angle $\tan^{-1} e$, and a vector along the y-axis which is deflected in counter-clockwise direction with the same angle. Therefore, distortion parameter shear is estimated by a shear angle. Similarly, for estimation of twist angle, the electric field vectors rotate through a clockwise angle $\tan^{-1} t$. RMS Error is a factor which indicates whether the MT data fits the distortion model with the acceptable value of RMS error or not. In Figure 7, the distortion parameters are calculated for various period bands as well as the broad period band. The maximum shear angle value observed for the period band 10-100s is 15.99°. Similarly, for twist angle, the maximum value observed for the period band 10-100s is 12.76°. Thus, for periods greater than 10s higher shear and twist values were observed, which could be the reason for the 3D structure shown in swift and Bahr skew results. However, the values of shear and twist angle for the broad period band is below +/-45°, which suggests a 2D structure. Thus, the distortion model fits the data with an acceptable average RMS error value of ~2°.

According to Simpson and Bahr (2005), induction arrows can be used to demarcate the presence or absence of lateral variations in conductivity, as these vertical magnetic fields are caused by lateral conductivity gradients. Induction arrows eliminate the 90° ambiguity cases, which helps in proper choice of regional strike direction. The induction arrow for the period band of 0.01 to 100sec is given in Figure 8. Westward and eastward pointing arrows, respectively

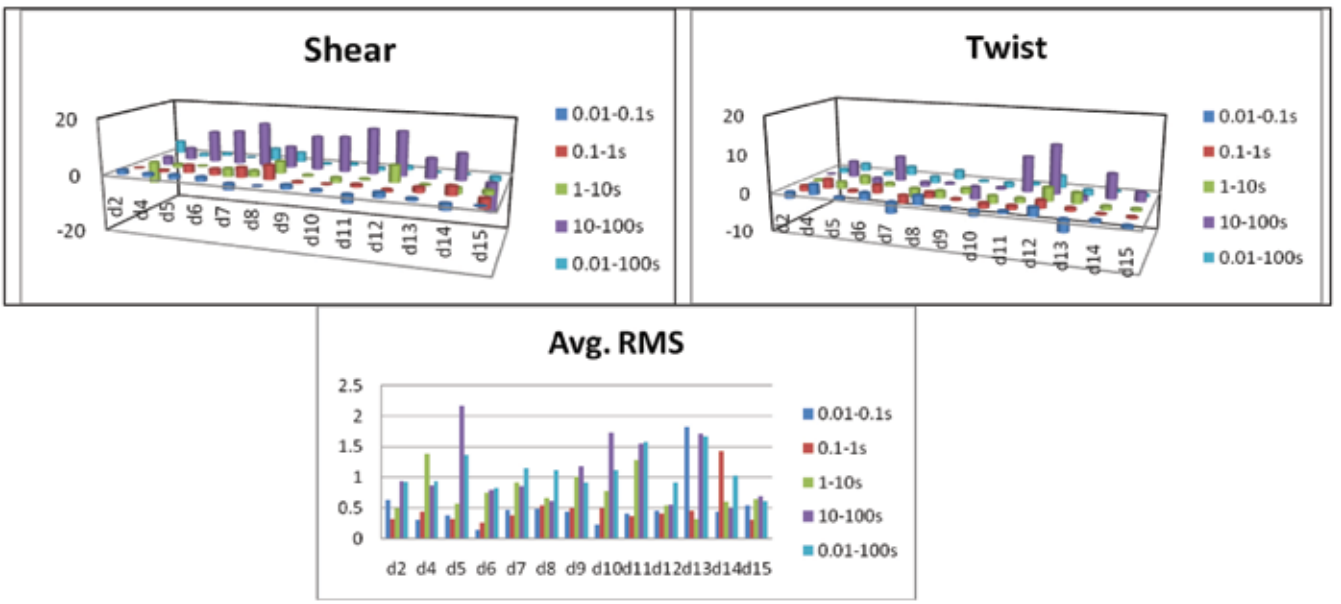

Figure 7. Distortion parameters plotted through GBD technique for various period bands as well as broad period band.

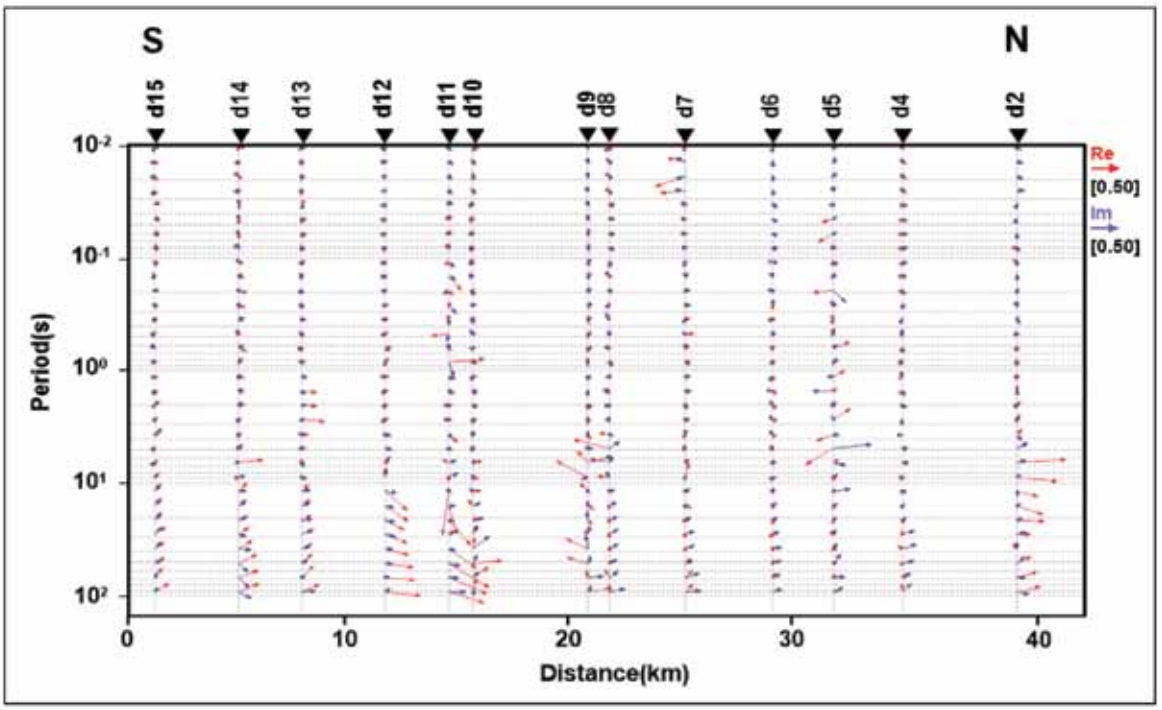

Figure 8. Induction arrow plot for broad period at each MT station.

indicate a zone of low resistivity that trends parallel to the strike direction (real arrows are oriented perpendicular to the electric strike). As expected, the real induction arrows point towards the conductive zone, present between the stations d9 and d10. Due to low resistive zone, the orientation of real induction arrows changes from east to west at station d9, also at station d2 the real induction arrows pointing towards the east, indicating a conductive zone. At increasing distance from the conductor the length of the arrows decreases. A sub-parallel alignment of the real arrows to their imaginary parts is another indication for a two-dimensional geometry (Rothe et al., 2004), which is observed at high periods (Figure 8).

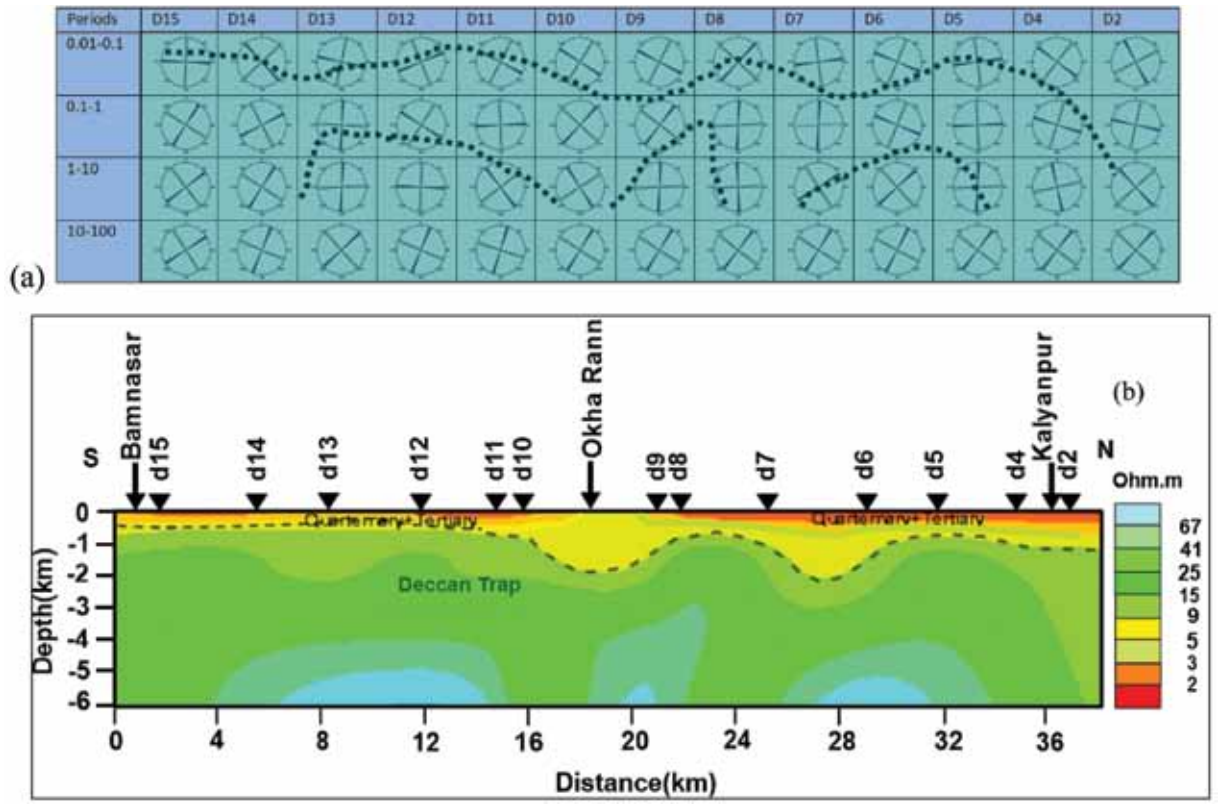

Figure 9. Correlation of (a) the estimated strike direction for various period bands at each site with (b) the 1D resistivity section generated from Occam's 1D inversion.

Correlation of strike with 1D model

A 1D smooth modeling approach is adopted for delineation of subsurface resistivity structure subjected to Occam's linearized scheme. The dimensionality analysis suggested 1D nature of data up to the 1s period. Therefore, 1D Occam inverse model up to 6 km depth is shown in Figure 9(b). The inverted model gave a resistivity value of <10 Ohm-m for Quaternary and Tertiary sediments and ~20 - 60 Ohm-m for Trap layer. The thickness of sediments is observed about 500m deep in the Southern part of the profile and increases to ~2km in the central part of the profile near Okha rann (Figure 9(b)). The thickness of sediments reduces to ~1km in the Northern part of the profile. The strike trend matches well with the 1D resistivity model. The NS strike direction is observed at station D5, D8 and D13 and also the undulations are clearly seen at the boundary of Quaternary-Tertiary sediments and Deccan trap in the 1D resistivity model (Figure 9(b)).

CONCLUSION

In the present study, the Dimensionality and Directionality analysis have been computed using Phase Tensor Analysis (PTA) technique, WALDIM Fortran code, Swift's and Bahr's Skew technique, Groom-Bailey (GB) and Becken and Burkhardt (BB) technique. Dimensionality parameters Swift skew and Bahr skew plots show 2D subsurface structure except some stations showing values greater than 0.3° for higher periods, which indicates the 3D subsurface structure. Because of heterogeneity present in the area, the skewness values are not same for all MT stations and for all period bands. The Phase Tensor analysis for all MT stations at four different bands shows moderate skewness values, except some stations which shows high skewness values suggesting the subsurface structure is more than 2D, the WALDIM results are consistent with Phase Tensor analysis results. The distortion model generated from the Groom and Bailey decomposition technique fits the data with RMS error value of ~2.0. Regional strike estimated through three techniques (PT, GB, and BB) suggests a NNE-SSW direction, consistent with the Delhi-Aravalli trend. From 1D resistivity model, the undulations are found at the boundary of Quaternary-Tertiary sediments and Deccan trap in the central and Northern part of the profile, which indicates the presence of faults.

ACKNOWLEDGEMENTS

We thank Director General and Director for their permission to publish the present work. This work is supported by

Gujarat Pavitra Yatradham Vikas Board (GPYVB). We are thankful to Prof. Alan G Jones and Prof. Becken and Burkhardt for providing strike decomposition codes.

Compliance with Ethical Standards

The authors declare that they have no conflict of interest and adhere to copyright norms.

REFERENCES

Bahr, K., 1988. Interpretation of the magnetotelluric impedance tensor: Regional induction and local telluric distortion, J. Geophys, 62, 119-127.

Bahr, K., 1991. Geological Noise in Magnetotelluric Data: A Classification of Distortion Types. Phys. Earth and Planet. Int.. 66, 24-38.

Barcelona et al., 2013. The potentials of audiomagnetotellurics in the study of geothermal fields: A case study from the northern segment of the La Candelaria Range, Northwestern Argentina. J. Appl. Geophys., 88, 83-93.

Becken, M. and Burkhardt, H., 2004. An Ellipticity criterion in Magnetotelluric tensor analysis. Geophys. J. Int., 159, 69-82

Berdichevsky, M.N., 1999. Marginal notes on magnetotellurics. Surv. Geophys., 20, 341-375.

Bhatt, N., 2000. Lithostratigraphy of neogene-quaternary deposits of Dwarka-Okha area, Gujarat. J. Geol. Soc. India. 55, 139-148.

Bibby, H.M., Caldwell, T.G. and Brown, C., 2005. Determinable and non-determinable parameters of Galvanic distortion in magnetotellurics. Geophys. J. Int., 163, 915-930.

Biswas, S.K., 1982. Rift basins in western margin of India and their hydrocarbon prospects with special reference to Kutch basin. Am. Assn. Petroleum Geol. Bull., 66, 307-327.

Biswas, S.K., 1987. Regional tectonic frame work, structure and evolution of the western marginal basins of India. Tectonophysics. 135, 307-327

Biswas, S.K., 2005. A review of structure and tectonics of Kutch basin, Western India, with special reference to earthquakes. Curr. Sci., 88(10), 1592-1600

Booker, 2014. The magnetotelluric phase tensor: A critical review. Surv. Geophys, 35, 7-40.

Caldwell, T.G., Bibby, H.M. and Brown, C., 2004. The Magnetotelluric phase tensor, Geophys. J. Int., 158, 457-469.

Febriani et al., 2017. The Magnetotelluric phase tensor analysis of the Sembalun Propak area, West Nusa Tenggara, Indonesia. J. Phys., conference series. 817: 012072

Groom, R.W. and Bailey, R.C., 1989. Decomposition of the Magnetotelluric impedance tensor in the presence of local three-dimensional galvanic distortion. J. Geophys. Res., 94, 1913-1925.

Heise et al., 2008. Three-dimensional modelling of Magnetotelluric data from the Rotokawa geothermal field, Taupo Volcanic Zone, New Zealand. Geophys. J. Int., 173, 740-750.

Hubert, 2012. From 2D to 3D models of electrical conductivity based upon Magnetotelluric data: Experiences from two case studies. Digital comprehensive summaries of Uppsala dissertations from the faculty of Science and Technology. 890:55

Jones and Groom, 1993. Strike-angle determination from the Magnetotelluric impedance tensor in the presence of noise and local distortion: rotate at your peril. Geophys. J. Int., 113, 524-534.

Jupp, D.L.B. and Vozoff, K., 1976. Stable iterative methods for the inversion of geophysical data. Geophysical J. Royal Astron. Soc., 42, 957-976.

Kashkouli et al., 2016. Dimensionality analysis of the subsurface structures in Magnetotellurics using different methods (a case study: oil field in Southwest of Iran). J. Mining. Environ, 7, 119-126.

Marti, A., Queralt, P. and Ledo, J., 2009. WALDIM: A code for the dimensionality analysis of magnetotelluric data using the rotational invariants of the magnetotelluric tensor. Comput. Geosci., 35:2295-2303

Marti et al., 2010. Dimensionality imprint of electrical anisotropy in Magnetotelluric responses. Phys. Earth planet. Int., 182(3-4), pp.139.

Marti et al., 2016. Magnetotelluric characterization of the Alhama de Murcia Fault (Eastern Betics) preliminary results. Near surface Geoscience. Conference and Exhibition.

McNeice, G.W. and Jones, A.G., 2001. Multisite, multifrequency tensor decomposition of magnetotelluric data. Conf. paper in Geophysics. 66, 158-173.

Mishra et al., 2001. Major lineaments and gravity-magnetic trends in Saurashtra, India. Curr. Sci., 80(8).

Naidu et al., 2011. Electrical signatures of the Earth's crust in central India as inferred from Magnetotelluric study. Earth Planets and Space. 63, 1175-1182.

Naidu, G.D., 2012. Deep Crustal Structure of the Son-Narmada-Tapti Lineament, Central India, Springer Thesis, DOI: 10.1007/978-3-642-28442-7_2.

Oskooi et al., 2013. Investigation of electrical resistivity and geological structures on the hot springs in Markazi province of Iran using Magnetotelluric method. Boll. Geof. Teor. Appl., 54, 245-256.

Patro et al., 2005. Electrical Imaging of Narmada-Son lineament zone, Central India from Magnetotellurics. Phys. Earth Planet. Int., 148, 215-232.

Patro et al., 2015. Sub-basalt sediment imaging-The efficacy of Magnetotellurics. J. Appl. Geophys., 121, 106-115.

Pandey, D.K., Bahadur, T. and Mathur, U.B., 2007. Stratigraphic distribution and depositional environment of the chaya formation along the Northwestern Coast of Saurashtra Peninsula, Western India. J. Geol. Soc. India. 69(6), 1215-1231.

Pranata et al., 2017. Magnetotelluric Data Analysis using Swift Skew, Bahr Skew, Polar Diagram and Phase Tensor: A Case Study in Yellowstone, US. A Physical and Computational Science. 54(3), 311-317.

Rothe et al., 2004. Correlation of electrical conductivity and structural damage at a major strike-slip fault in Northern Chile. J. Geophys. Res., 109.

Selway et al., 2012. A simple 2D explanation for the negative phases in TE Magnetotelluric data. Geophysical J. Int., 188, 945-958.

Sharma et al., 2004. Delineation of electrical structure beneath Saurashtra peninsula using MT studies. 5th Conference and Exposition on Petroleum Geophysics, Hyderabad, India. 79-80.

Singh, S.B. et al., 2004. Delineation of Basaltic covered sediments in the Saurashtra region using Deep Resistivity Sounding studies. 5th Conference and Exposition on petroleum geophysics, Hyderabad. 69-74.

Simpson, F. and Bahr, K., 2005. Practical Magnetotellurics. Cambridge University Press, Cambridge, 270 pp.

Subbarao, P.B.V., Singh, A.K. and Rao, C.K., 2012. Regional conductance map of Saurashtra and surrounding regions. Curr. Sci., 103(2).

Swift, C.M., 1967. A magnetotelluric investigation of an electrical conductivity anomaly in the South Western of United States. Ph.D. Thesis. Massachusetts Institute of Technology.

Tao et al., 2010. Refined processing and two-dimensional inversion of Magnetotelluric data I: Impedance tensor decomposition and analysis of structural dimensionality. Chinese J. Geophys., 53, 6

Vozoff, K., 1972. The magnetotelluric method in the exploration of sedimentary basins. Geophys., 37, 98-141.

Weaver, J.T., Agarwal, A.K. and Lilley, F.E.M., 2000. Characterization of the Magnetotelluric in terms of its invariants. Geophys.J. Int., 141, 321-336.

Wiese, H., 1962. Geomagnetische... Teil II: Die streichrichtung der Untergrundstrukturen des elektrischen Widerstandes, erschlossen aus geomagnetischen variationen. Geo□.s Pura et Appl. 52, 83-103.

Yadav et al., 2008. Probabilistic assessment of earthquake hazard in Gujarat and adjoining regions. Pure Appl. Geophys., 165, 1813-1833.

Received on: 14.6.18; Revised on: 21.9.18; Accepted on: 1.10.18